PHYSICAL REVIEW C, VOLUME 62, 064311

Dissociation of ^{8}He

Y. Iwata* and K. Ieki
Department of Physics, Rikkyo University, 3 Nishi-Ikebukuro, Toshima, Tokyo 171-8501, Japan

A. Galonsky, J. J. Kruse,† J. Wang,‡ R. H. White-Stevens,§ E. Tryggestad, and P. D. Zecher‖
National Superconducting Cyclotron Laboratory and Department of Physics and Astronomy, Michigan State University, East Lansing, Michigan 48824-1321

F. Deák, Á. Horváth, and Á. Kiss
Department of Atomic Physics, Eötvös Loránd University, Pázmány P. sétány 1/A, H-1117 Budapest, Hungary

Z. Seres
KFKI Research Institute for Particle and Nuclear Physics, Konkoly-Thege út 29-33, P.O. Box 49, H-1525 Budapest 114, Hungary

J. J. Kolata, and J. von Schwarzenberg
Department of Physics, University of Notre Dame, Notre Dame, Indiana 46556

R. E. Warner
Department of Physics, Oberlin College, Oberlin, Ohio 44074

H. Schelin
CEFET, Av. Sete de Setembro 3165 80230-901, Curitiba, Pr, Brazil
(Received 16 June 2000; published 15 November 2000)

We have performed kinematically complete measurements of dissociation of ^{8}He into ^{6}He and two neutrons at $E/A = 24$ MeV. The targets were Sn and Pb. A prominent peak around 0.4 MeV in the relative energy distribution of the $^6\mathrm{He}+n$ system is consistent with the ground state of ^{7}He, suggesting sequential decay via ^{7}He in ^{8}He dissociation. Further evidence of the sequential decay was found in neutron momentum distributions. The excitation energy distributions of ^{8}He were reconstructed. For the Sn target, it shows a peak which is suggestive of the first excited state of ^{8}He ($E_x = 3.6$ MeV, $\Gamma = 0.5$ MeV, and $J^\pi = 2^+$). The distribution for the Pb target was found to have a broad structure, indicating the $E1$ continuum, as observed in measurements of other halo nuclei. The photonuclear cross section $\sigma_{E1}(E_x)$ and the dipole strength function $dB(E1)/dE_d$ were deduced for the first time. The integrated dipole strength up to 3 MeV decay energy is 0.091 ± 0.026 $e^2\mathrm{fm}^2$. Insignificant energy-weighted strength, compared to the cluster sum rule, indicates that ^{8}He does not have the $^6\mathrm{He}+2n$ structure. Agreement of the measured neutron momentum distributions with the COSMA model is in favor of the $^4\mathrm{He}+4n$ structure.

PACS number(s): 25.70.De, 21.10.Gv, 25.60.Gc, 27.20.+n

I. INTRODUCTION

The recent development of radioactive nuclear beams has led us to explore structures and reactions of nuclei far from stability. One of the most intriguing features in studies of light neutron-rich nuclei is the neutron halo structure represented by ^{11}Li. Subsequent measurements have led to the discovery of this structure in ^{6}He, ^{8}He [1,2] and heavier nuclei.

Besides the conspicuous halo nucleus ^{11}Li, intensive studies have been made on ^{6}He due to its relatively simple structure—described as a ^{4}He core and two neutrons. On the other hand, less attention has been paid to ^{8}He because the structure is considered to be more complicated. Owing to weak binding of the ^{6}He nucleus, ^{8}He cannot be regarded as having a ^{6}He core surrounded by two valence neutrons. The ^{4}He nucleus still exists as a core without large modification of its wave function. Therefore, ^{8}He might rather have the structure of $^4\mathrm{He}+4n$. The two-neutron separation energy of ^{8}He (S_{2n}= 2.14 MeV) is only somewhat larger than that of ^{6}He (S_{2n}= 0.975 MeV), in spite of the fact that ^{8}He has a completely filled $1p_{3/2}$ neutron shell. This small difference in S_{2n} values is also suggestive of the $^4\mathrm{He}+4n$ structure.

*Present address: National Institute of Radiological Sciences, 4-9-1 Anagawa, Inage, Chiba 263-8555, Japan. Electronic address: y_iwata@nirs.go.jp

†Present address: Radiation Oncology, Mayo Clinic, 200 First St. SW, Rochester, MN 55905.

‡Present address: American Express Co., 3WFC, 4712B, 200 Vesey Street, New York, NY 10285.

§Present address: Department of Physics, University of Notre Dame, Notre Dame, IN 46556.

‖Present address: Investor Analytics LLC, 630 Fifth Avenue Suite 1919, New York, NY 10111.

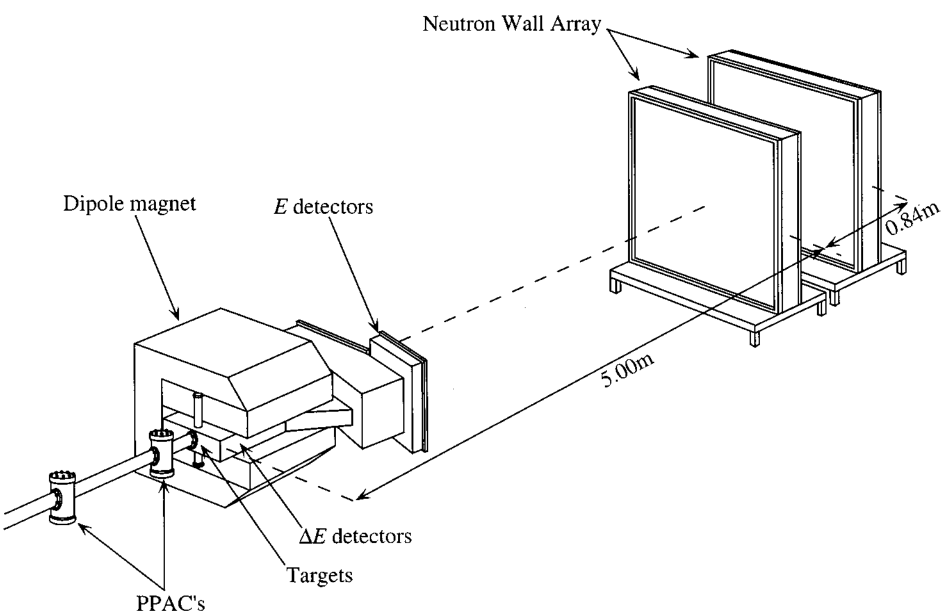

FIG. 1. A schematic drawing of the detector setup. The fragment detectors consisting of Si-strip ΔE detectors and plastic E detectors are installed in a vacuum chamber. The *Neutron Wall Array* is centered at zero degrees along the beam axis.

Evidence of the $^4\mathrm{He}+4n$ structure was also found from the measurements of interaction cross sections. According to the Glauber model, the $2n$-removal cross section σ_{-2n} and the interaction cross section σ_I should satisfy the relation $\sigma_{-2n}(^8\mathrm{He})=\sigma_I(^8\mathrm{He})-\sigma_I(^6\mathrm{He})$ if ^{6}He and ^{8}He are both $2n$ halo nuclei [3]. However, the experimental cross sections do not satisfy this relation, but instead satisfy a relation $\sigma_{-2n}(^8\mathrm{He})+\sigma_{-4n}(^8\mathrm{He})=\sigma_I(^8\mathrm{He})-\sigma_I(^4\mathrm{He})$, indicating the $4n$ halo structure [4].

The ^{8}He nucleus is intriguing because its neutron-to-proton ratio is the largest among known bound nuclei. The ground state ($J^\pi=0^+$) has a dominant configuration of the ^{4}He core ($J^\pi=0^+$) and four valence neutrons in the $1p_{3/2}$ shell. Moreover, excited states were found in several measurements [5–7]. The spin-parity of the first excited state is assigned as $J^\pi=2^+$, which is in good agreement with shell-model calculations [8–10]. The configuration of this is understood to be $(1p_{3/2})^{-1}\ (1p_{1/2})^1$, just as for the 2^+ state in ^{12}C.

An interesting property of some halo nuclei is the existence of a low-lying, unbound excitation. While most of the dipole strength for stable nuclei is known to be exhausted by a giant dipole resonance with excitation energies $E_x \simeq 78A^{-1/3}$, an enhancement of the dipole strength at $E_x \simeq 1$ MeV was first observed in ^{11}Li [11–13]. Furthermore, this excitation mode also was observed in the halo nuclei ^{11}Be [14] and ^{6}He [15]. To explain it, a new collective mode, called a soft dipole resonance, was proposed [16].

Measurements of this low-lying excitation are important to clarify the collective structure in halo nuclei. However, no experimental study has yet been dedicated to the ^{8}He nucleus. Recently, measurements of breakup reactions of ^{8}He on C and Pb targets at $E/A=240$ MeV have been performed [17,18]. Although the excitation energy distribution of ^{8}He was reconstructed, no crucial information on the low-lying excitation was presented.

In order to clarify the interpretation of the low-lying excitation of ^{8}He, we have performed a kinematically complete measurement of Coulomb dissociation of ^{8}He on a Pb target at $E/A=24$ MeV. To accomplish this, momenta of the outgoing decay products, ^{6}He and two neutrons, from the dissociation of ^{8}He were measured in coincidence. In addition, a measurement with Sn target has been performed to evaluate the contribution of nuclear dissociation. The kinematically complete measurements allowed us to reconstruct an excitation energy distribution of ^{8}He and momentum distributions of ^{6}He and neutrons in the ^{8}He rest frame. With the measured excitation energy distributions, we have deduced a photonuclear cross section and a dipole strength function for the first time.

II. EXPERIMENT

The experiment was performed at the National Superconducting Cyclotron Laboratory (NSCL) in Michigan State University. A secondary beam of ^{8}He was produced by utilizing projectile fragmentation reactions of an $^{18}\mathrm{O}^{6+}$ primary beam having $E/A=80$ MeV on a 1.9 g/cm^2 Be production target. Then, the ^{8}He beam was analyzed, separated with the A1200 Fragment Separator [19], and degraded to $E/A=25$ MeV before being transported to the experimental vault. The energy dispersion of the beam, defined by momentum slits of the A1200, was set to $(\Delta p/p)=1\%$ corresponding to $(\Delta E/A)$ = 0.5 MeV in energy. The average intensity of the ^{8}He beam was a few hundred particles/s, corresponding to 15% of the total number of beam particles. The major impurity of the beam was 85% ^{12}Be at $E/A=44$ MeV. Events originating from impurity beam particles were distinguished with fragment detectors.

A schematic drawing of the experimental setup is shown in Fig. 1. Before ^{8}He projectiles impinged on a target, their incident angle and position on target were measured with two position-sensitive parallel plate avalanche counters (PPAC's) located upstream from the target. In the experiment, we used targets of Al (247 mg/cm^2), Sn (364 mg/cm^2), and Pb (397 mg/cm^2). After ^{8}He dissociation into ^{6}He$+2n$ in the target, the momentum of the decay product ^{6}He was measured with fragment detectors consisting of a ΔE detector and an E detector [20]. The ΔE detector was composed of two 250-μm position-sensitive silicon double-strip detectors with lateral dimensions 5 cm $\times$5 cm; each has 16 horizontal strips on one side and 16 vertical strips on the other. The two detectors were located 15.4 cm downstream from the target and were installed side by side, giving 32 (horizontal) $\times$ 16 (vertical) square pixels for position information. The emission angle of the ^{6}He was determined by the pixel that it traversed and the PPAC data on the incident ^{8}He. The geometrical angular acceptance of the ΔE detectors is $\pm 18.2°$ (horizontal) and $\pm 9.3°$ (vertical). The corresponding ^{6}He momenta after the target are $|p_x| \leqslant 390$ MeV/c (horizontal) and $|p_y| \leqslant 200$ MeV/c (vertical). Furthermore, energy loss information in the detector was used for particle identification.

After passing through the ΔE detector, the ^{6}He was deflected by the dipole magnet and stopped in the E detector, which consisted of 16 vertically-arranged bars of Bicron BC-408 plastic scintillator. Light produced in these scintillation detectors was collected with two photomultipliers attached to the top and bottom ends of each bar. The ^{6}He energy was determined by the light intensity. Since the light-output response of the plastic scintillator is a nonlinear function of fragment energy and also depends on the mass and charge of the fragment, a semiempirical formula was used to determine the energy of the fragment [21]. To determine free parameters in the formula, calibrations were made for various isotopes at several energies. As a result, the systematic error of the energy calibration for the He isotopes was found to be less than 1%.

The particle identification of charged fragments was accomplished with Si ΔE and plastic E signals from the fragment detectors. Figure 2 shows two-dimensional ΔE-E distributions: 2(a) for an E signal in any of the 16 bars; 2(b) for an E signal in only one bar. A coincidence with at least one neutron was required. The abscissa shows energy per nucleon for ^{6}He particles. As the light response of the plastic scintillator depends on the incident isotope, in general, the energy scale is not correct for particles other than ^{6}He.

Since ^{8}He hits mostly one bar, those data are included in the upper, but not the lower figure. In Fig. 2(a), two groups are seen. One group shows the locus of ^{8}He and ^{6}He particles, and it has a horizontal tail to lower energies; most of those events have the same ΔE, but different E's. When ^{8}He dissociates in the E detector, the Si ΔE signal is the same as that for a dissociation in the target, while the energy deposition in the E detector is lower, as neutrons carry out some energy. Hence, the tail is attributed to ^{8}He dissociation events in the E detector. The plastic E of the other group is higher than that of the ^{8}He beam. When the energy scale is normalized for ^{4}He, the energy of the group is about $E/A \simeq 40$ MeV. Thus these ^{4}He are produced in dissociation reactions of $E/A = 44$ MeV ^{12}Be particles, which are the major impurity of the incident beam.

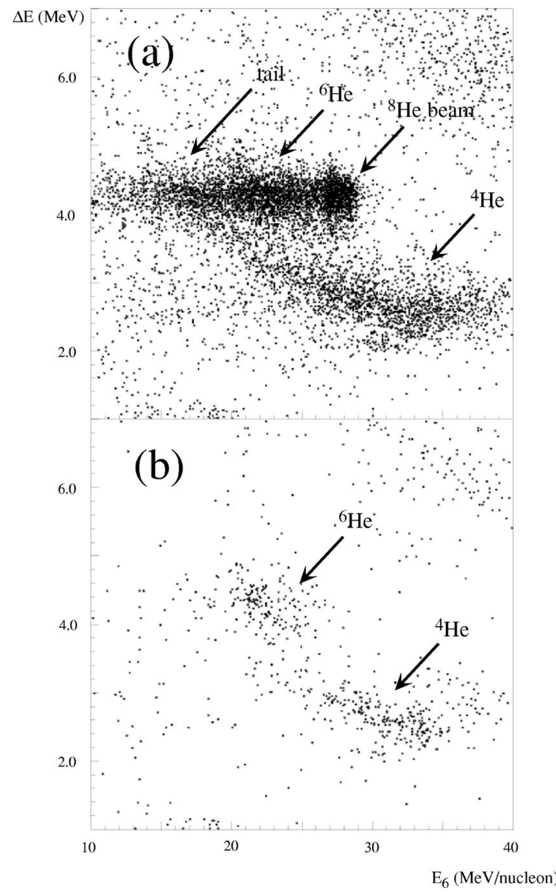

FIG. 2. Two-dimensional distributions of Si ΔE versus plastic E in which a coincidence with at least one neutron was required for (a) the sum of the 16 scintillators and (b) only one scintillator of the E detectors. The abscissa is normalized for ^{6}He in units of MeV/nucleon (see text).

With our detector setup, the fragments having different rigidities are separated by the dipole magnet, and therefore clear particle identification was accomplished with the ΔE-E distributions for the individual scintillator bars. Figure 2(b) shows a ΔE-E distribution for a bar not hit by the ^{8}He. Instead of the horizontal tail, a group corresponding to ^{6}He particles at $E/A \simeq 22$ MeV is clearly seen.

The momentum of each neutron was determined with the *Neutron Wall Array*. The array has two walls, each with 25, 2-m-long rectangular glass cells filled with NE-213 liquid scintillator and with phototubes at the ends. The two walls were placed at 5 m and 6 m downstream from the target location. Since most of the neutrons from the ^{8}He dissociation are emitted at forward angles, the walls were centered at zero degrees. Because of the limited vertical opening angle of the dipole magnet, the 16 cells in the central region for each wall were used. The geometrical angular acceptance of neutrons is $\pm 11.3°$ (horizontal) and $\pm 6.8°$ (vertical), corresponding to $|p_x| \leqslant 42$ MeV/c and $|p_y| \leqslant 25$ /c for 24 MeV neutrons, respectively. With pulse-shape information from the NE213, neutron/γ-ray discrimination was made for each cell of the walls. Position and time resolutions of each cell were better than 10 cm and 1 ns, respectively. A detailed description of the *Neutron Wall Array* is given in Ref. [22].

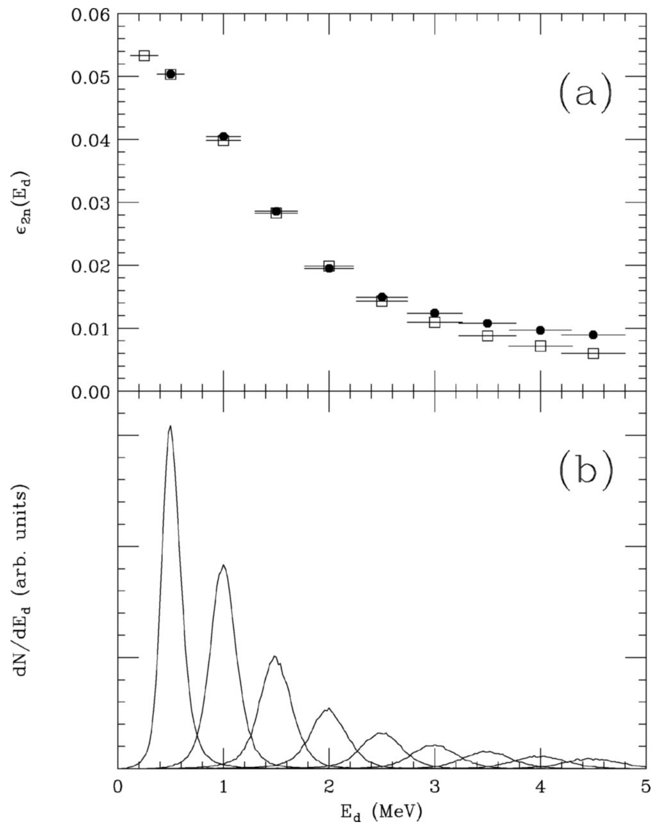

FIG. 3. (a) Calculated overall acceptance $\epsilon_{2n}(E_d)$ of the total detector system for ^{6}He$+2n$ coincidences as a function of the decay energy E_d. Filled circles and open squares show results assuming the sequential and direct decay model, respectively. (b) Decay energy distributions calculated for fixed decay energies. The distributions reflect the resolution of the total detector system for the respective decay energy.

The overall acceptance and resolution of the total detection system for the ^{6}He$+2n$ coincidence were estimated by Monte Carlo simulations. The simulations include all contributions of effects from the beam spreads in energy, angle and position on target, from target thickness, multiple scattering in the target, geometrical acceptance, and intrinsic resolutions and efficiencies of the detectors. To describe the ^{8}He dissociation, we adopted sequential and direct decay models. A detailed description of those models is presented in the following sections. The calculated overall acceptance $\epsilon_{2n}(E_d)$ according to the sequential and direct decay models as functions of decay energy E_d (excitation energy above the two neutron emission threshold) is shown by the filled circles and the open squares in Fig. 3(a), respectively. We see that the acceptance differs more and more as the decay energy increases.

To estimate the overall resolution, decay energy distributions were calculated for fixed decay energies $E_d = 0.5$–4.5 MeV in 0.5 MeV steps as shown in Fig. 3(b). Those distributions reflect the overall resolution for the respective decay energies. Since the distributions assuming the two models are identical, only those of the sequential decay model are presented. The typical resolution is found to be about 0.38 MeV (FWHM) at $E_d = 1$ MeV and roughly proportional to the square root of the decay energy.

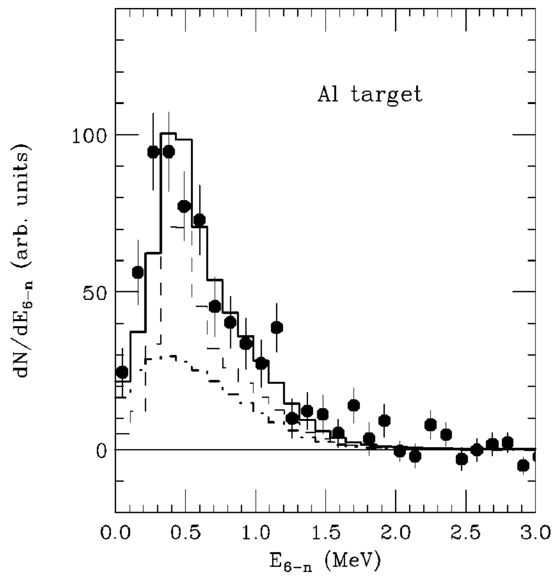

FIG. 4. Relative energy distribution of ^{6}He$+n$ system for the Al target. The points are the experimental data. The solid histogram shows the results of Monte Carlo calculations assuming 60% sequential decay via the intermediate state of ^{7}He$+n$ (dashed histogram) with 40% admixture of the direct decay process (dot-dashed histogram).

III. RESULTS

A. Sequential decay via ^{7}He

The relative energy distribution of the ^{6}He$+n$ system for the Al target is provided in Fig. 4. The distribution has a prominent peak around 0.4 MeV, which corresponds to the ground state of ^{7}He, suggesting sequential decay via ^{7}He in the ^{8}He dissociation [23]. In the sequential decay, the neutron of ^{8}He would be largely scattered out or stripped by the target nucleus and therefore not be detected. Since this process leads to a depression of the neutron multiplicity, apparent $2n$-removal cross section determined from inclusive data (^{6}He$+n$) would differ from that determined from exclusive data (^{6}He$+2n$). In fact we found the difference. From the cross sections, the sequential process was estimated to occupy approximately $60\pm10\%$ of the total for the Al target, which is comparable to that of Ref. [18], and approximately $40\pm20\%$ for the Sn and Pb targets. Since the process is attributed to the nuclear interaction and the ratio of the nuclear interaction to the Coulomb interaction decreases as the target charge increases, the process is relatively less important for the heavier targets.

To describe the measured relative energy distribution, a model calculation with a Monte Carlo simulation was performed. First, we assumed 60% of the ^{8}He dissociation proceeds via the intermediate state of ^{7}He. Since ^{7}He is unstable with respect to neutron emission by 0.44 MeV, the ^{7}He nucleus subsequently decays into ^{6}He$+n$ with a Breit-Wigner (BW) function given by

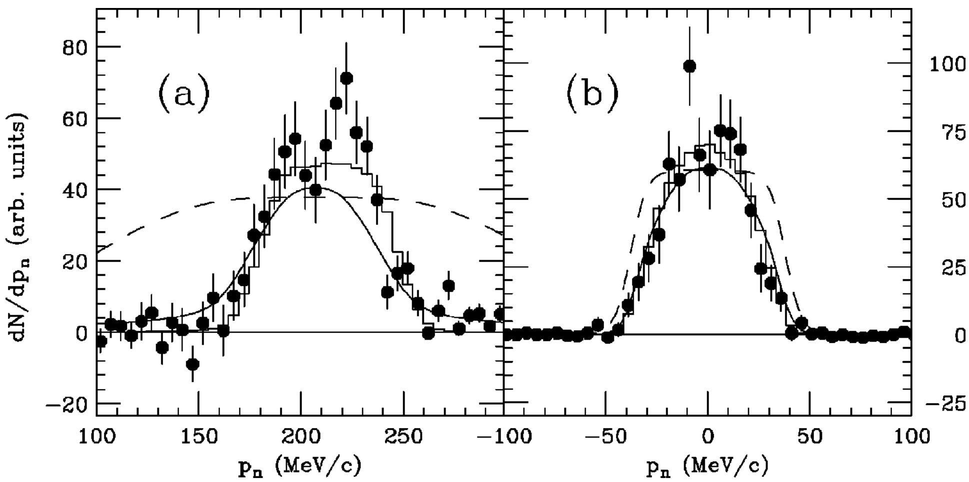

FIG. 5. (a) Longitudinal and (b) transverse components of neutron momentum distributions in coincidence with the ^{6}He fragment for the Al target. Histograms show results of the Monte Carlo simulation assuming 60% sequential decay via the intermediate state of ^{7}He$+n$ with 40% admixture of the direct decay process. The solid and dashed curves show results of the model calculation (COSMA) with and without a correction for the final state interaction (FSI) of the ^{7}He resonance, respectively.

$$I_{\mathrm{BW}}(E_{6-n}) \propto \frac{1}{2\pi} \frac{\Gamma(E_{6-n})}{(E_{6-n}-E_0)^2+(\Gamma(E_{6-n})/2)^2}, \tag{1}$$

$$\Gamma(E_{6-n}) = \Gamma_0 \frac{T(E_{6-n})}{T(E_0)}, \tag{2}$$

where E_{6-n} is the relative energy of the ^{6}He$+n$ system, and the resonant energy E_0 and the width Γ_0 are taken to be 0.44 and 0.16 MeV, respectively, corresponding to the ground state of ^{7}He [24]. The width $\Gamma(E_{6-n})$ is energy dependent; a transmission coefficient of p-wave neutrons $T(E_{6-n})$ was used. Next, we assumed the other 40% of the dissociation proceeds via the first excited state of ^{8}He. A detailed description of the decay via the first excited state is presented in the next section. Then, the relative energy distribution was calculated with a Monte Carlo simulation, and the result is shown by the solid histogram in Fig. 4. In addition, the results of each component—the dissociation via the intermediate state of ^{7}He and via the first excited state of ^{8}He—are shown by the dashed and dot-dashed histograms in the figure, respectively. The prominent peak around 0.4 MeV corresponding to the ^{7}He ground state was fairly well reproduced by the simulation.

Further evidence in favor of sequential decay was found in neutron momentum distributions. Transverse and longitudinal components of the neutron momentum distributions for the Al target are displayed in Fig. 5. The histograms in the figure show results of the Monte Carlo simulation described above. The momentum distributions are in good agreement with the simulation.

Recently, a simple five-body cluster orbital shell model approximation (COSMA) has been proposed [25,26] and extended to the case of ^{8}He in order to describe the ^{8}He ground state wave function [27–29]. It was demonstrated that momentum distributions of several experiments were reproduced with those calculated by the COSMA with sequential decay [18,27–29]. We therefore adopted the prescription of the COSMA calculation. Calculated distributions according to the COSMA wave function with and without considering the final state interaction (FSI) of the ^{7}He resonance are shown in Fig. 5 by the solid and dashed curves, respectively. Note that the calculations included the acceptance of the detector system. As shown in the figure, the calculated distributions which include the FSI reproduce the experimental distributions, while those without it do not. This indicates that the distributions were significantly modified by the FSI and lost information on the ground state wave function of ^{8}He. We therefore conclude that sequential decay is the leading reaction in the dissociation of ^{8}He by Al.

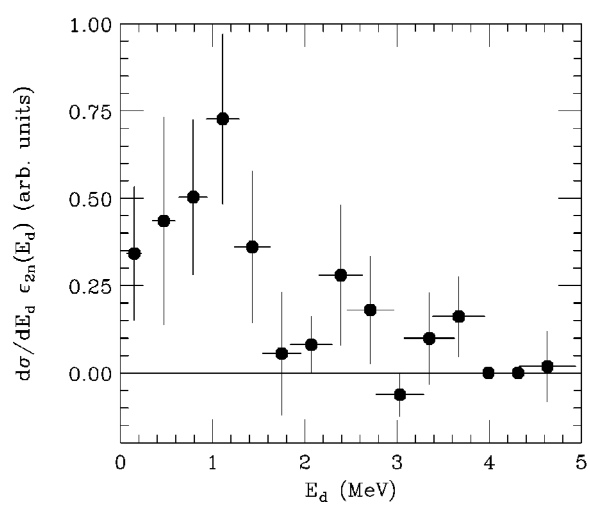

FIG. 6. Measured ^{8}He decay energy distribution for the Sn target. The function $\epsilon_{2n}(E_d)$ refers to the overall acceptance of the total detector system for the ^{6}He$+2n$ coincidence as a function of the decay energy E_d [see Fig. 3(a)]. A peak around $E_d \simeq 1$ MeV corresponding to the first excited state of ^{8}He is observed in the distribution.

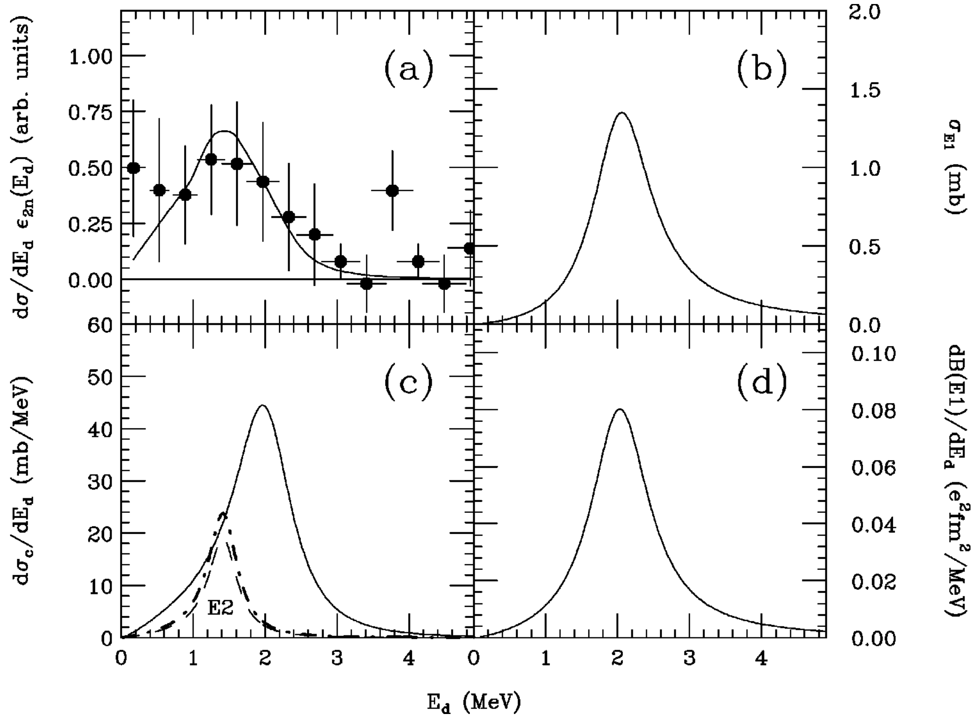

FIG. 7. The points are the measured ^{8}He decay energy distribution for the Pb target. The function $\epsilon_{2n}(E_d)$ refers to the overall acceptance of the total detector system for the $^6\mathrm{He}+2n$ coincidence as a function of the decay energy E_d [see Fig. 3(a)]. (a) The solid curve shows a good fit of the calculated distribution to the experimental data obtained by varying parameters of a Breit-Wigner function for σ_{E1}. (b) Photonuclear cross section σ_{E1}. (c) $E1$ Coulomb dissociation cross section $d\sigma_c/dE_d$. The dashed and dot-dashed curves show the $E2$ Coulomb dissociation cross section estimated by single particle calculations (see text). The magnitudes of the dashed and dot-dashed curves are multiplied by 10^3 and 10, respectively. (d) Dipole strength function $dB(E1)/dE_d$.

B. Coulomb excitation of ^{8}He

With the kinematically complete measurements, the continuum excitation energy of ^{8}He can be reconstructed. False $2n$ cross-talk events were rejected off-line [30]. The excitation energy E_x is related to the decay energy E_d by $E_x = E_d + S_{2n}$, where S_{2n} (=2.14 MeV) is the separation energy of two neutrons. The measured decay energy distributions for the Sn and Pb targets are shown in Figs. 6 and 7(a), respectively. Data from the target with the highest Z, the Pb target, offer the best opportunity to study the Coulomb excitation of ^{8}He. But even in Pb there will be some nuclear excitation which we must take into account in determining the Coulomb excitation. To make a quantitative estimate of the nuclear excitation, we adopted the factorization of the nuclear dissociation cross section σ_{nucl} as in [31]

$$\sigma_{\mathrm{nucl}} = \gamma_P \gamma_{PT}, \tag{3}$$

$$\gamma_{PT} = R_I(P) + R_I(T), \tag{4}$$

where γ_P is a length which is the same for all targets, $R_I(P) = 2.48 \pm 0.03$ fm [1] for the ^{8}He projectile and $R_I(T) = 7.66$ fm for the Pb target. On the other hand, the Coulomb dissociation cross section σ_{Coul} was assumed to have the form

$$\sigma_{\mathrm{Coul}} = \alpha Z_{\mathrm{T}}^2, \tag{5}$$

where α is a constant and Z_{T} is the target charge number. The Coulomb dissociation cross sections of the Pb and Sn targets were fitted with $\sigma_{\mathrm{nucl}} + \sigma_{\mathrm{Coul}}$, and we obtained the parameters $\gamma_P = 0.910$ fm and $\alpha = 0.0132$ mb. With these parameters, the Coulomb and nuclear dissociation cross sections were determined to be 89 and 92 mb for the Pb target; 33 and 80 mb for the Sn target, respectively. The nuclear contribution probably comes via inelastic scattering to the 2^+ first-excited state, which is at 3.6 MeV ($E_d = 1.46$ MeV) with a width of 0.5 MeV [5,6]. With the factorization, the approximately 70% excitation for the Sn target is attributed to the nuclear contribution, and the shape of the Sn spectrum in Fig. 6 is suggestive of such an excitation mode. Therefore we assume that all the nuclear excitation in Pb occurs via this mode. To describe the nuclear dissociation, we employed a BW function in which the width and resonant parameters were taken to be those of the 2^+ state, namely, $E_0 = 1.46$ MeV and $\Gamma_0 = 0.50$ MeV. The normalization of the resonance was determined by the factorization.

Although various multipolarities contribute to the nonresonant Coulomb dissociation, the $E1$ mode is expected to dominate. The $E1$ strength has been observed to be considerably larger than the $E2$ strength in both ^{11}Li [11–13] and ^{11}Be [14] dissociation, and $E1$ population of the continuum has been observed in recent measurements of the breakup of ^{6}He at $E/A = 240$ MeV into $^4\mathrm{He}+2n$ on a Pb target [15]. Furthermore, it is shown in Sec. IV B that $E2$ Coulomb excitation of the first excited state is negligible. To evaluate the

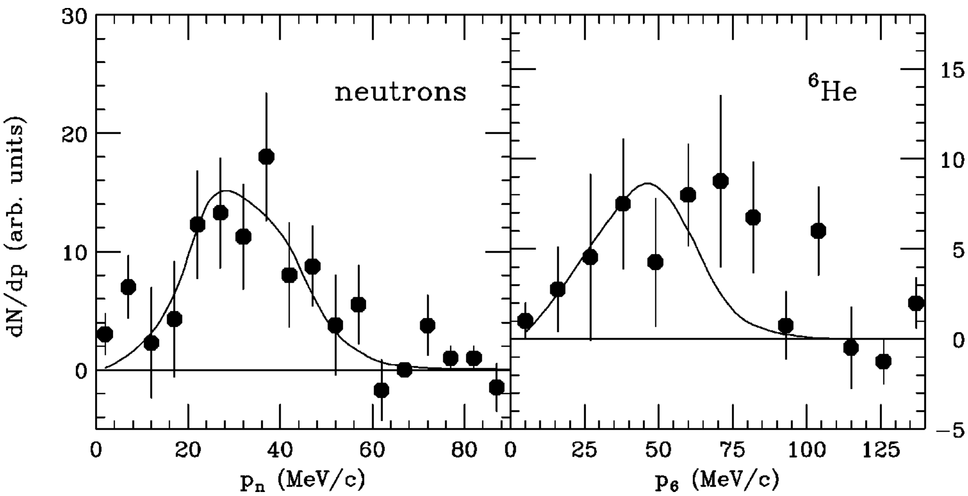

FIG. 8. Momentum distributions of neutrons (p_n) and ^{6}He (p_6) in the rest frame of ^{8}He for the Pb target. The solid curves show the result of a Monte Carlo simulation (see text).

$E1$ strength here, we assumed that ^{8}He is excited into the $E1$ continuum and then decays with the 3-body phase space distribution into ^{6}He and two neutrons. We parametrized the $E1$ photonuclear cross section $\sigma_{E1}(E_x)$ with another BW function characterized by a resonant energy E_0^{Coul} and a width Γ_0^{Coul} which is energy dependent as described in Eqs. (1) and (2).

The Coulomb dissociation cross section $d\sigma_c/E_x$ is related to the photonuclear cross section σ_{E1} by

$$\frac{d\sigma_c}{dE_x}=n_{E1}(E_x)\frac{\sigma_{E1}(E_x)}{E_x}, \tag{6}$$

where the function $n_{E1}(E_x)$ is the virtual photon density for an electric dipole [32]. With this relation, the Coulomb dissociation cross section for the electric dipole contribution can be calculated once E_0^{Coul} and Γ_0^{Coul} are selected. Monte Carlo simulations with variation of these two parameters were performed. The fixed nuclear contribution and the detector response function were included. A good fit to the experimental distribution yielded $E_0^{\text{Coul}}=2.1$ MeV and $\Gamma_0^{\text{Coul}}=1.0$ MeV for the BW of $\sigma_{E1}(E_x)$. That fit is shown by the solid curve in Fig. 7(a), and $\sigma_{E1}(E_x)$ vs E_d is in Fig. 7(b). Having included the detector response in the fit, we can use Eq. (6) to determine the true function $d\sigma_c/dE_x$ vs E_d, and that is given in Fig. 7(c). Finally, the dipole strength function can be calculated with the relation

$$\frac{dB(E1)}{dE_x}=\frac{9\hbar c}{16\pi^3}\frac{1}{n_{E1}(E_x)}\frac{d\sigma_c}{dE_x} \tag{7}$$

and that function is shown in Fig. 7(d). By integrating the solid curve in Fig. 7(d) up to $E_d=3$ MeV, we obtained the $E1$ strength $B(E1)=0.091\pm0.026\,e^2\text{fm}^2$.

In Fig. 8, momentum distributions of neutrons (p_n) and of ^{6}He (p_6) in the ^{8}He rest frame are presented. Results of the Monte Carlo simulations described previously are shown by the solid curves in the figures. For the Coulomb dissociation, the decay energy was assumed to be partitioned between ^{6}He and neutrons according to the three-body phase space distribution. On the other hand, sequential decay via the intermediate state of ^{7}He was assumed for the nuclear dissociation.

IV. DISCUSSION

A. Sum rules

From the measured decay energy distribution, the dipole strength function was derived. The energy-weighted dipole strength for the Pb target S_{expt}^{E1} is determined by

$$S_{\text{expt}}^{E1}=\int E_x\frac{dB(E1)}{dE_x}dE_x \tag{8}$$

and is listed in Table I. By integrating the solid curve in Fig. 7(d) to infinity, we got $S_{\text{expt}}^{E1}=0.50\pm0.14\,e^2\text{fm}^2$ MeV.

For isovector dipole transitions, the total strength can be evaluated with the Thomas-Reiche-Kuhn (TRK) sum rule as

$$S_{\text{TRK}}^{E1}\equiv\sum_f (E_f-E_i)B(E1;i\rightarrow f) \tag{9}$$

$$=\frac{9}{4\pi}\frac{\hbar^2}{2M}\frac{ZN}{A}e^2, \tag{10}$$

where i and f refer to the initial and final states, respectively; Z, N and A are those of ^{8}He; and M is the nucleon mass. The sum includes all of the possible continuum. The TRK sum is also listed in Table I. The experimental sum S_{expt}^{E1} was found to be $2.3\pm0.6\%$ of that calculated by the TRK sum rule.

TABLE I. Values of energy-weighted sums. The experimental value S_{expt}^{E1} was extracted from the Pb target. The S_{TRK}^{E1} and the $S_{^6\text{He-}2n}^{E1}$ were calculated with the Thomas-Reiche-Kuhn (TRK) sum rule and the cluster sum rule, respectively.

Quantity	$\Sigma_f(E_f-E_i)B(E1;i\rightarrow f)$ ($e^2\text{fm}^2$ MeV)
S_{expt}^{E1}	0.50 ± 0.14
S_{TRK}^{E1}	22
$S_{^6\text{He-}2n}^{E1}$	2.5

Assuming that the ^{8}He has a clusterlike structure, i.e., a bound dineutron system coupled to a ^{6}He core, one may decompose the total energy-weighted sum $S^{E1}_{\rm tot}$ for the electric dipole as $S^{E1}_{\rm tot}=S^{E1}_{^6{\rm He}}+S^{E1}_{2n}+S^{E1}_{^6{\rm He}\text{-}2n}$, where $S^{E1}_{^6{\rm He}}$, S^{E1}_{2n}, and $S^{E1}_{^6{\rm He}\text{-}2n}$ refer to the sum rule for the core, the dineutron, and the relative motion between the two clusters, respectively [33,34]. Assuming the individual clusters are not excited, the total sum for the electric dipole is attributed to that of the relative motion of the two clusters. Using Eq. (10), the sum rule for the relative motion $S^{E1}_{^6{\rm He}\text{-}2n}$ can be evaluated as

$$S^{E1}_{^6{\rm He}\text{-}2n}=\frac{9}{4\pi}\frac{\hbar^2}{2M}\frac{N_{2n}Z^2_{^6{\rm He}}}{AA_{^6{\rm He}}}e^2 \tag{11}$$

This limit is also listed in Table I. The experimental sum $S^{E1}_{\rm expt}$ is 20$\pm$5% of the cluster sum. On the other hand, the model predicts a sum equal to 2.7 $e^2{\rm fm}^2$ MeV for the structure ^{9}Li$+2n$ for ^{11}Li, and the data [11,13] are consistent with this value. This comparison supports the idea that ^{8}He does not have a ^{6}He core.

B. Contribution of the $E2$ Coulomb excitation

In order to evaluate the contribution of $E2$ strength to Coulomb excitation of the 2^+ state of ^{8}He, the strength was estimated by the single particle calculation. Since the state has the configuration of $(1p_{3/2})^{-1}(1p_{1/2})^1$, the $E2$ strength for the single particle transition $B_{\rm sp}(E2)$ is given by

$$B_{\rm sp}(E2)=\frac{5}{4\pi}e^2\left\langle j_i\frac{1}{2}20\middle| j_f\frac{1}{2}\right\rangle^2\langle j_f|r^2|j_i\rangle^2, \tag{12}$$

where $j_i(=3/2)$ and $j_f(=1/2)$ refer to spins of the initial and the final state, respectively. For a neutron transition, a recoil effect of the rest of the nucleus was considered. To estimate the order of magnitude of the effect, the effective charge, given by $e^{\rm recoil}_{E2}=(Z/A^2)e$, was used. With the COSMA wave function [27], the strength was estimated to be $B^{\rm recoil}_{\rm sp}(E2)=0.011\,e^2{\rm fm}^4$.

By using this $E2$ strength, the Coulomb dissociation cross section $d\sigma_c/dE_d$ can be calculated. The shape of $d\sigma_c/dE_d$ was determined by Eq. (6) for with $E2$ replacing $E1$ and with the BW type photonuclear cross section $\sigma_{E2}(E_x)$. The parameters of the BW function were taken to be $E_0=1.46$ MeV and $\Gamma=0.50$ to describe the first excited state. Since the Coulomb dissociation cross section $d\sigma_c/dE_x$ is related to the $E2$ strength function $dB(E2)/dE_x$ by

$$\frac{dB(E2)}{dE_x}=\frac{75}{4}\left(\frac{\hbar c}{\pi}\right)^3\frac{1}{n_{E2}(E_x)}\frac{1}{E_x^2}\frac{d\sigma_c}{dE_x} \tag{13}$$

the magnitude of $d\sigma_c/dE_d$ was determined so that the integration of Eq. (13) yields the calculated $E2$ strength $B^{\rm recoil}_{\rm sp}(E2)$. The result is shown by the dashed curve in Fig. 7(c). We see that the $E2$ strength is more than 3 orders of magnitude smaller than the $E1$ strength.

In Ref. [35], the effective charge of the $E2$ strength for p-shell nuclei was calculated to be $e_n=0.35e$, about 10 times the recoil value. By using this, we obtain the $E2$ strength $B_{\rm sp}(E2)=1.4e^2{\rm fm}^4$, and the calculated Coulomb dissociation cross section is shown by the dot-dashed curve in Fig. 7(c). As seen in the figure, we may say that the $E2$ strength is insignificant; most of the excitation is attributed to the $E1$ strength as discussed previously.

V. SUMMARY AND CONCLUSIONS

We have performed kinematically complete measurements of the dissociation of ^{8}He into ^{6}He and two neutrons at E/A = 24 MeV. Those measurements allowed us to provide crucial information on the reaction mechanism and on the presence of the $E1$ continuum excitation in the ^{8}He dissociation.

First, we have confirmed the sequential decay mode, $^8{\rm He}\rightarrow{}^7{\rm He}+n$, in the ^{8}He dissociation. A clue to this mode was found in the relative energy distribution of the ^{6}He$+n$ system. With the $2n$-removal cross sections extracted from inclusive and exclusive data sets, we found significant sequential decay—approximately 60$\pm$10% for the Al target and approximately 40$\pm$20% for the Sn and Pb targets. A peak at $E_{6-n}\simeq0.4$ MeV for the Al target was reproduced with a Monte Carlo simulation assuming 60% sequential decay and 40% direct decay.

Further evidence of the sequential decay was found in neutron momentum distributions determined from the ^{6}He $+n$ coincidence data with the Al target. These distributions were also reproduced with 60% sequential decay. In addition, we found that the calculated neutron momentum distributions according to the COSMA wave function with the FSI of ^{7}He reproduced the measured distributions. We therefore concluded that the main part of the dissociation may be attributed to the sequential decay process via ^{7}He.

A peak in the decay energy distribution for the Sn target was suggestive of the known first excited state of ^{8}He. On the other hand, the distribution for the Pb target has a rather broad structure, indicating $E1$ excitation into the continuum. By assuming that the $E1$ photonuclear cross section function $\sigma_{E1}(E_x)$ is parametrized with the Breit-Wigner function, the measured decay energy distribution was well reproduced. The best fit to the measured distribution yields the parameters of the function $E_0^{\rm Coul}=2.1$ MeV and $\Gamma_0^{\rm Coul}=1.0$ MeV. With these parameters, we have deduced, for the first time, and for the first 2–3 MeV of decay energy E_d, the decay energy distribution $d\sigma_c/dE_d$, the photonuclear cross section σ_{E1}, the dipole strength function $dB(E1)/dE_d$ and the integrated value $B(E1)$. Insignificant energy-weighted strength, compared to the cluster sum rule, indicates that ^{8}He does not have the ^{6}He$+2n$ structure. Instead, agreement of our measured distributions with the five-particle COSMA model is in favor of the structure ^{4}He core$+4n$.

ACKNOWLEDGMENTS

We thank V. Zelevinsky for helpful discussions; J. Yurkon, D. Swan, and J. Vincent for their technical assistance and R. Fox for his support of the data acquisition system. Support of the U.S. National Science Foundation under Grant Nos. PHY94-23659, PHY94-24149, and INT-13997, of the Hungarian Science Foundation under OTKA Grant No. T16059, of the Bolyai Janos Research Foundation, of the Ministry of Education, Science, Sports and Culture of Japan under Grant Nos. 08044095 and 08640392 and of the Japan Society for the Promotion of Science is gratefully acknowledged.

[1] I. Tanihata, H. Hamagaki, O. Hashimoto, Y. Shida, K. Sugimoto, O. Yamakawa, T. Kobayashi, and N. Takahashi, Phys. Rev. Lett. **55**, 2676 (1985).

[2] M. J. G. Borge, P. G. Hansen, L. Johannsen, B. Jonson, T. Nilsson, G. Nyman, A. Richter, K. Rissager, O. Tengblad, K. Wilhelmesen, and the ISOLDE Collaboration, Z. Phys. A **340**, 255 (1991).

[3] Y. Ogawa, K. Yabana, and Y. Suzuki, Nucl. Phys. **A543**, 722 (1992).

[4] I. Tanihata, D. Hirata, T. Kobayashi, S. Shimoura, K. Sugimoto, and H. Toki, Phys. Lett. B **289**, 261 (1992).

[5] A. A. Korsheninnikov, K. Yoshida, D. V. Aleksandrov, N. Aoi, Y. Doki, N. Inabe, M. Fujimaki, T. Kobayashi, H. Kumagai, C. B. Moon, E. Yu. Nikolsky, M. M. Obuti, A. A. Ogloblin, A. Ozawa, S. Shimoura, T. Suzuki, I. Tanihata, Y. Watanabe, and M. Yanokura, Phys. Lett. B **316**, 38 (1993).

[6] W. von Oertzen, H. G. Bohlen, B. Gebauer, M. von Lucke-Petsh, A. N. Ostrowski, Ch. Seyfert, Th. Stolla, M. Wilpert, Th. Wilpert, D. V. Alexandrov, A. A. Koresheninnikov, I. Mukha, A. A. Ogloblin, R. Kalpakchieva, Y. E. Penionzhkevich, S. Piskor, S. M. Grimes, and T. N. Massey, Nucl. Phys. **A588**, 129c (1995).

[7] Th. Stolla, H. G. Bohlen, B. Gebauer, S. M. Grimes, R. Kalpakchieva, T. N. Massey, W. von Oertzen, A. N. Ostrowski, M. Wilpert, and Th. Wilpert, Z. Phys. A **356**, 233 (1996).

[8] N. A. F. M. Poppelier, A. A. Wolters, and P. W. M. Glaudemans, Z. Phys. A **346**, 11 (1993).

[9] N. A. F. M. Poppelier, L. D. Wood, and P. W. M. Glaudemans, Phys. Lett. **157B**, 120 (1985).

[10] P. Navrátil and B. R. Barrett, Phys. Rev. C **57**, 3119 (1998).

[11] K. Ieki, D. Sackett, A. Galonsky, C. A. Bertulani, J. J. Kruse, W. G. Lynch, D. J. Morrissey, N. A. Orr, H. Schulz, B. M. Sherril, A. Sustich, A. Winger, F. Deák, Á. Horváth, Á. Kiss, Z. Seres, J. J. Kolata, R. E. Warner, and D. L. Humphrey, Phys. Rev. Lett. **70**, 730 (1993).

[12] D. Sackett, K. Ieki, A. Galonsky, C. A. Bertulani, H. Esbensen, J. J. Kruse, W. G. Lynch, D. J. Morrissey, N. A. Orr, B. M. Sherril, H. Schulz, A. Sustich, A. Winger, F. Deák, Á. Horváth, Á. Kiss, Z. Seres, J. J. Kolata, R. E. Warner, and D. L. Humphrey, Phys. Rev. C **48**, 118 (1993).

[13] S. Shimoura, T. Nakamura, M. Ishihara, N. Inabe, T. Kobayashi, T. Kubo, R. H. Siemssen, I. Tanihata, and Y. Watanabe, Phys. Lett. B **348**, 29 (1995).

[14] T. Nakamura, S. Shimoura, T. Kobayashi, T. Teranishi, K. Abe, N. Aoi, Y. Doki, M. Fujimaki, N. Inabe, N. Iwasa, K. Katori, T. Kubo, H. Okuno, T. Suzuki, I. Tanihata, Y. Watanabe, A. Yoshida, and M. Ishihara, Phys. Lett. B **331**, 296 (1994).

[15] T. Aumann, D. Aleksandrov, L. Axelsson, T. Baumann, M. J. G. Borge, L. V. Chulkov, J. Cub, W. Dostal, B. Eberlein, Th. W. Elze, H. Emling, H. Geissel, V. Z. Goldberg, M. Golovkov, A. Grünshloss, M. Hellström, K. Henchen, J. Holeczek, R. Holzmann, B. Jonson, A. A. Korshenninikov, J. V. Kratz, G. Kraus, R. Kulessa, Y. Leifels, A. Leistenschneider, T. Leth, I. Mukha, G. Münzenberg, F. Nickel, T. Nilsson, G. Nyman, B. Petersen, M. Pfützner, A. Richter, K. Riisager, C. Scheidenberger, G. Schrieder, W. Schwab, H. Simon, M. H. Smedberg, M. Steiner, J. Stroth, A. Surowiec, T. Suzuki, O. Tengblad, and M. V. Zhukov, Phys. Rev. C **59**, 1252 (1999).

[16] K. Ikeda, Nucl. Phys. **A538**, 355c (1992).

[17] T. Nilsson, F. Humbert, W. Schwab, M. Zinser, Th. Blaich, M. J. G. Borge, L. V. Chulkov, H. Eickhoff, Th. W. Elze, H. Emling, B. Franzke, H. Freiesleben, H. Geissel, K. Grimm, D. Guillemaud-Mueller, P. G. Hansen, R. Holzmann, H. Irnich, L. Johannsen, B. Jonson, J. G. Keller, O. Klepper, H. Klingler, J. V. Kratz, R. Kulessa, D. Lambrecht, Y. Leifels, A. Magel, M. Mohar, E. F. Moore, A. C. Muller, G. Münzenberg, P. Møller, F. Nickel, G. Nyman, A. Richter, K. Riisager, C. Scheidenberger, G. Schrieder, B. M. Sherrill, H. Simon, K. Stelzer, J. Stroth, O. Tengblad, W. Trautmann, E. Wajda, and E. Zude, Nucl. Phys. **A593**, 795 (1995).

[18] T. Nilsson, F. Humbert, W. Schwab, H. Simon, M. H. Smedberg, M. Zinser, Th. Blaich, M. J. G. Borge, L. V. Chulkov, Th. W. Elze, H. Emiling, H. Geissel, K. Grimm, D. Guillemaud-Mueller, P. G. Hansen, R. Holtzmann, H. Irnich, B. Jonson, J. G. Keller, H. Klingler, A. A. Korsheninnikov, J. V. Kratz, R. Kulessa, D. Lambrecht, Y. Leifels, A. Magel, M. Mohar, A. C. Mueller, G. Münzenberg, F. Nickel, G. Nyman, A. Richter, K. Riisager, C. Scheidenberger, G. Schrieder, B. M. Sherrill, K. Stelzer, J. Stroth, O. Tengblad, W. Trautmann, E. Wajda, M. V. Zhukov, and E. Zude, Nucl. Phys. **A598**, 418 (1996).

[19] B. M. Sherrill, D. J. Morrissey, J. A. Nolen, and J. A. Winger, Nucl. Instrum. Methods Phys. Res. B **56&57**, 1106 (1991).

[20] J. J. Kruse, A. Galonsky, C. Snow, E. Tryggestad, J. Wang, K. Ieki, Y. Iwata, and P. D. Zecher, Nucl. Instrum. Methods Phys. Res. A (to be published).

[21] D. Fox, D. R. Bowman, G. C. Ball, A. Galindo-Uribarri, E. Hagberg, D. Horn, L. Beaulieu, and Y. Larochelle, Nucl. Instrum. Methods Phys. Res. A **374**, 63 (1996).

[22] P. D. Zecher, A. Galonsky, J. J. Kruse, S. J. Gaff, J. Ottarson, J. Wang, F. Deák, Á. Horváth, Á. Kiss, Z. Seres, K. Ieki, Y. Iwata, and H. Schelin, Nucl. Instrum. Methods Phys. Res. A **401**, 329 (1997).

[23] T. Kobayashi, in *Proceedings of the Third International Conference on Radioactive Nuclear Beams*, edited by D. J. Morrissey (Editions Frontieres, Gif-sur-Yvette, 1993), p. 169.

[24] F. Ajzenberg-Selove, Nucl. Phys. **A598**, 418 (1996).

[25] M. V. Zhukov and D. V. Fedorov, Yad. Fiz. **53**, 5621 (1991) [Sov. J. Nucl. Phys. **53**, 351 (1991)].

[26] M. V. Zhukov, D. V. Danilin, D. V. Fedorov, J. M. Band, I. J. Thompson, and J. S. Vaagen, Phys. Rep. **231**, 151 (1993).

[27] M. V. Zhukov, A. A. Korsheninnikov, and M. H. Smedberg, Phys. Rev. C **50**, R1 (1994).
[28] M. V. Zhukov, A. A. Korsheninnikov, M. H. Smedberg, and T. Kobayashi, Nucl. Phys. **A583**, 803 (1995).
[29] A. A. Korsheninnikov, M. V. Zhukov, M. H. Smedberg, and T. Kobayashi, Europhys. Lett. **29**, 359 (1995).
[30] J. Wang, A. Galonsky, J. J. Kruse, P. D. Zecher, F. Deák, Á. Horváth, Á. Kiss, Z. Seres, K. Ieki, and Y. Iwata, Nucl. Instrum. Methods Phys. Res. A **397**, 380 (1997).
[31] D. L. Olson, B. L. Berman, D. E. Greiner, H. H. Heckman, P. J. Lindstrom, and H. J. Crawford, Phys. Rev. C **28**, 1602 (1983).
[32] C. A. Bertulani and G. Baur, Phys. Rep. **163**, 299 (1988).
[33] Y. Alhassid, M. Gai, and G. F. Bertsch, Phys. Rev. Lett. **49**, 1482 (1982).
[34] H. Sagawa and M. Honma, Phys. Lett. B **251**, 17 (1990).
[35] A. G. M. van Hees and P. W. M. Glaudemans, Z. Phys. A **315**, 223 (1984).